NAD^+ supplementation reduces neuroinflammation and cell senescence in a transgenic mouse model of Alzheimer's disease via cGAS–STING

Yujun Hou[a,b], Yong Wei[a,c], Sofie Lautrup[a,d], Beimeng Yang[a], Yue Wang[a], Stephanie Cordonnier[a], Mark P. Mattson[e], Deborah L. Croteau[a], and Vilhelm A. Bohr[a,f,1]

[a]Section on DNA Repair, National Institute on Aging, NIH, Baltimore, MD 21224; [b]Institute for Regenerative Medicine, Shanghai East Hospital, Shanghai Key Laboratory of Signaling and Disease Research, School of Life Sciences and Technology, Tongji University, Shanghai 200092, People's Republic of China; [c]Hubei Key Laboratory of Cell Homeostasis, College of Life Sciences, Wuhan University, Wuhan 430072, People's Republic of China; [d]Department of Clinical Molecular Biology, University of Oslo and Akershus University Hospital, 1478 Lørenskog, Norway; [e]Department of Neuroscience, Johns Hopkins University School of Medicine, Baltimore, MD 21205; and [f]Danish Center for Healthy Aging, University of Copenhagen, Copenhagen 2200, Denmark

Edited by Fred H. Gage, Salk Institute for Biological Studies, La Jolla, CA, and approved July 23, 2021 (received for review June 1, 2020)

Alzheimer's disease (AD) is a progressive and fatal neurodegenerative disorder. Impaired neuronal bioenergetics and neuroinflammation are thought to play key roles in the progression of AD, but their interplay is not clear. Nicotinamide adenine dinucleotide (NAD^+) is an important metabolite in all human cells in which it is pivotal for multiple processes including DNA repair and mitophagy, both of which are impaired in AD neurons. Here, we report that levels of NAD^+ are reduced and markers of inflammation increased in the brains of APP/PS1 mutant transgenic mice with beta-amyloid pathology. Treatment of APP/PS1 mutant mice with the NAD^+ precursor nicotinamide riboside (NR) for 5 mo increased brain NAD^+ levels, reduced expression of proinflammatory cytokines, and decreased activation of microglia and astrocytes. NR treatment also reduced NLRP3 inflammasome expression, DNA damage, apoptosis, and cellular senescence in the AD mouse brains. Activation of cyclic GMP-AMP synthase (cGAS) and stimulator of interferon genes (STING) are associated with DNA damage and senescence. cGAS–STING elevation was observed in the AD mice and normalized by NR treatment. Cell culture experiments using microglia suggested that the beneficial effects of NR are, in part, through a cGAS–STING-dependent pathway. Levels of ectopic (cytoplasmic) DNA were increased in APP/PS1 mutant mice and human AD fibroblasts and down-regulated by NR. NR treatment induced mitophagy and improved cognitive and synaptic functions in APP/PS1 mutant mice. Our findings suggest a role for NAD^+ depletion-mediated activation of cGAS–STING in neuroinflammation and cellular senescence in AD.

Alzheimer's disease | inflammation | DNA repair | neurodegeneration | NAD supplementation

Alzheimer's disease (AD) is the most feared neurodegenerative disease and is characterized by progressive cognitive impairment associated with extensive accumulation of amyloid β-peptide (Aβ) plaques and tau neurofibrillary tangles in vulnerable brain regions (1, 2). There are no available treatments. Neuroinflammation, mitochondrial dysfunction, and cellular senescence have been recognized as key drivers of AD (3–6). Microglia are the primary innate immune cells in the brain. Although accumulating evidence challenges the simplified M1-M2 phenotypes of microglia, the classification is still widely in use as microglia can be protective (M2) and detrimental (M1) under different circumstances (7, 8). The detrimental microglia are activated by Aβ and produce interleukin (IL)-1β, TNF-α, and other proinflammatory molecules. The protective microglia secrete the anti-inflammatory cytokines IL-4 and IL-10 (8).

The inflammatory response is one of the hallmarks of cellular senescence (9). The senescence-associated secretory phenotype (SASP) includes cessation of cell division and the production of proinflammatory cytokines (10). The SASP is highly correlated with neuroinflammation and has been documented in the brains of AD mouse models (11). During normal aging, the number of senescent cells in tissues increases significantly (10), and evidence suggests that microglia, astrocytes, and oligodendrocyte progenitor cells can become senescent in AD (5, 11, 12). Moreover, senolytic treatments can preserve cognitive function in AD mice (11). However, the mechanisms that result in neuroinflammation and cell senescence in AD remain unclear.

Nicotinamide adenine dinucleotide (NAD^+) plays a central role in cellular metabolism and is also critical for maintaining mitochondrial homeostasis and genome integrity (13). Emerging evidence has identified lower levels of NAD^+ in affected tissues in many neurodegenerative diseases, including AD (13–16). Supplementation with the NAD^+ precursor nicotinamide riboside (NR) efficiently increases NAD^+ and can have beneficial effects on many AD features in mouse models (14). The cyclic GMP-AMP synthase (cGAS)–STING (stimulator of interferon genes) DNA-sensing pathway detects the presence of cytosolic DNA and triggers expression of inflammatory genes that lead to senescence or to the activation of defense mechanisms (17–20). Here, we explore the mechanisms by which NAD^+ supplementation reduces neuroinflammation and cell senescence in AD. Our results suggest that the cGAS–STING pathway is a therapeutic target for AD.

Significance

Impaired neuronal bioenergetics and neuroinflammation are thought to play key roles in the progression of Alzheimer's disease (AD), but their interplay is not clear. AD mouse brains showed lower nicotinamide adenine dinucleotide (NAD^+) levels and alterations in inflammation. Treatment of AD mice with NR reduced neuroinflammation, attenuated DNA damage, and prevented cellular senescence. We present evidence that the beneficial effects of nicotinamide riboside (NR) are, in part, through a cyclic GMP-AMP synthase (cGAS)–stimulator of interferon genes (STING)-dependent pathway. DNA damage was increased in AD and attenuated by NR. Both cGAS–STING and NAD^+ pathways are potential therapeutic targets for AD.

Author contributions: Y.H., Y. Wei, S.L., B.Y., Y. Wang, D.L.C., and V.A.B. designed research; Y.H., Y. Wei, S.L., B.Y., Y. Wang, S.C., and D.L.C. performed research; S.C., M.P.M., and D.L.C. contributed new reagents/analytic tools; Y.H., B.Y., and V.A.B. analyzed data; and Y.H., S.L., Y. Wang, M.P.M., D.L.C., and V.A.B. wrote the paper.

Competing interest statement: V.A.B. has a Cooperative Research and Development Agreement (CRADA) with Chromadex Corporation but receives no personal benefits.

This article is a PNAS Direct Submission.

[1]To whom correspondence may be addressed. Email: vbohr@nih.gov.

This article contains supporting information online at https://www.pnas.org/lookup/suppl/doi:10.1073/pnas.2011226118/-/DCSupplemental.

Published September 8, 2021.

Results

Neuroinflammation Increases and NAD$^+$ Levels Decrease with Age in the Brains of AD Mice. We performed unbiased gene expression microarray analysis on hippocampi and cerebral cortex from 12-mo-old APP/PS1 AD mice and their wild-type (WT) littermates. Gene ontology (GO) terms showed that the terms most altered in AD mice hippocampi were related to inflammation (Fig. 1 *A* and *B*). The GO terms with the highest normalized enrichment scores were immune response, chemokine activity, and inflammatory response, all significantly up-regulated in AD compared to WT (Fig. 1*A*). This suggests that inflammation is markedly elevated in the hippocampus of AD mice at this age. The following genes had the largest normalized enrichment score changes: *Cst7*, *Clec7a*, *Itgax*, *Ccl3*, and *Ccl6* (Fig. 1*B*); and were all related to inflammation, immunity, and microglia (21). Confirming these findings, analysis of Kyoto Encyclopedia of Genes and Genomes (KEGG), Reactome, and Biocarta functional categories revealed that the most significantly altered processes were also inflammation related (*SI Appendix*, Fig. S1*A*). Similarly, microarray analysis from cerebral cortex samples showed that the most changed GO terms and genes were inflammation related when comparing AD mice with WT mice (*SI Appendix*, Fig. S1 *B* and *C*). This supports an important role for neuroinflammation and microglia in the pathogenesis of AD.

In order to investigate the progression of neuroinflammation in AD mice, we used AD and WT mice at 3, 7, 12, or 20 mo of age. Inflammasomes are intracellular multiprotein complexes composed of NOD-like receptors (NLRs)/AIM-like receptors, the NLR family, pyrin domain containing 3 (NLRP3), absent in melanoma 2 (AIM2), containing pyrin domain containing 1 (NLRP1), and caspase activation recruitment domain containing 4 (NLRC4) and are critical factors in response to proinflammatory stimuli. The NLRP3 inflammasome is a cytosolic signaling complex that is mainly expressed in microglia and plays a role in their inflammatory responses (22). The main function of the NLRP3 inflammasome is the identification of products of damaged cells. Recent studies have found that NLRP3 is abnormally activated in AD and that it plays an important role in its pathology (23, 24). NLRP3 expression was significantly higher in the cortex of 12-mo-old AD mice than in WT (Fig. 1 *C* and *D*). AIM2 has been implicated in AD and aging and is responsive to microglial DNA damage (25). However, our results showed that AIM2, NLRP1, and NLRC4 inflammasomes were not significantly changed in the cortex of AD mice, compared

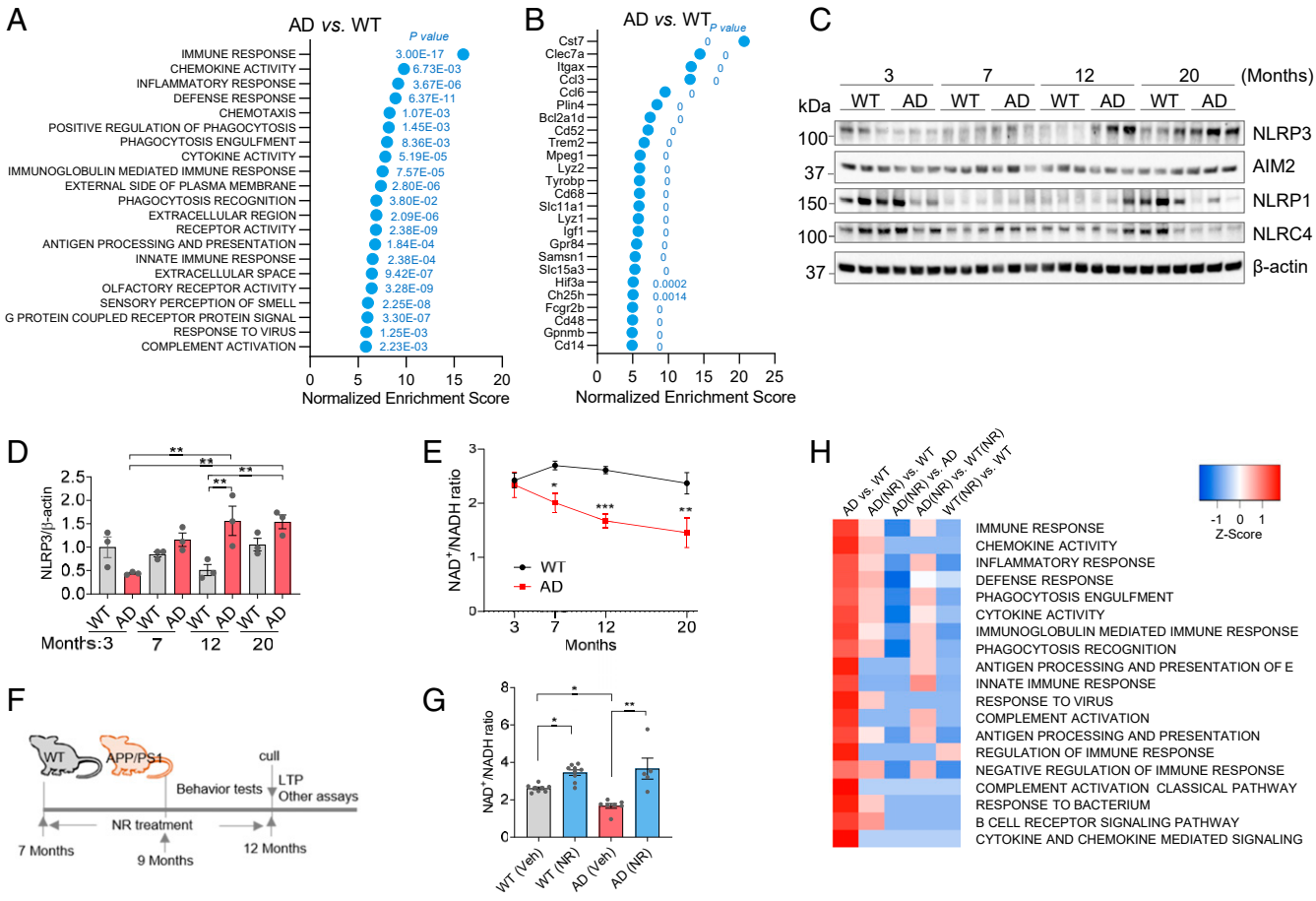

Fig. 1. Neuroinflammation is associated with reduced NAD$^+$ levels during aging in AD mice. (*A*) GO term analysis of gene expression microarray from hippocampi. The most changed terms in AD compared to WT hippocampus are shown. *P* values for each significant changed pathway are shown. (*B*) The most changed genes from hippocampi microarray of AD compared to WT. *P* values for each significant changed gene are shown. (*C*) Western blots of specific inflammation-related proteins at different ages from cortical tissue from WT and APP/PS1 mice. $n = 3$ mice per group. (*D*) Quantification of NLRP3 protein level in *C*. (*E*) NAD$^+$/NADH ratio in different ages of AD and WT mouse cortex. $n = 3$ to 8 mice per group. (*F*) Experimental design. The 7-mo-old AD and WT mice were treated with NR (12 mM) in their drinking water or vehicle for 5 mo. Behavioral tests were performed after 2 mo NR treatment. Mice were culled after 5 mo on NR or vehicle treatment for downstream assays. (*G*) NAD$^+$/NADH ratio in 12-mo-old AD and WT mouse cortex with or without NR treatment. $n = 5$ to 9 mice per group. (*H*) Microarray heatmap showing significantly changed inflammation-related pathways in NR- or vehicle-treated AD or WT mice hippocampus. Data: mean ± SEM. Statistical significance was performed with two-way ANOVA followed by Tukey's multiple comparisons test compared with control. $^*P < 0.05$, $^{**}P < 0.01$, $^{***}P < 0.001$.

to WT mice (Fig. 1*C* and *SI Appendix*, Fig. S2 *A–C*). Estimation statistics are included for data visualization. The mean differences and the CIs were calculated, and the effect sizes are estimated. In addition to the classical significance testing, we also show the estimation statistics for Fig. 1*C* (*SI Appendix*, S2 *D–G*). Accumulating studies show that the ability of Aim2/AIM2 proteins to exert pro- and anti-inflammatory effects in the central nervous system (CNS) may depend upon age, sex hormones, cell types, and the expression of species-specific negative regulators of the Aim2/AIM2 inflammasome (25). AIM2 expression is age dependent, this may be a reason why we did not see the expression difference between two genotypes, as they are both old mice. The array data showed marked increase in neuroinflammation. The phenotypic characterization of APP/PS1 AD mice showed that early amyloid plaques, gliosis, and cognitive impairment occur and are evident by 12 mo in these mice (*SI Appendix*, Fig. S2*H*) (26–28).

The NAD^+/NADH ratio was decreased in the cerebral cortex of AD mice at 7, 12, and 20 mo, compared to WT mice (Fig. 1*E*). We treated mice with the NAD^+ precursor NR (12 mM in drinking water) at 7 mo of age and onwards and began behavioral experiments after 2 mo of treatment. Cerebral cortex and hippocampus tissues were collected after 5 mo of treatment (Fig. 1*F*), and the NAD^+/NADH ratio was significantly elevated in the cerebral cortex of NR-treated AD mice compared to vehicle-treated mice (Fig. 1*G* and *SI Appendix*, Fig. S2 *I* and *J*). Gene expression analysis from hippocampus showed that almost all inflammation-related pathways were significantly down-regulated in the AD mice after NR treatment (Fig. 1*H*), suggesting that NR dramatically reduces neuroinflammation.

NR Decreases Neuroinflammation and DNA Damage. To further investigate the effects of NR on neuroinflammation in the brains of APP/PS1 mice, we performed immunostaining quantifying GFAP and IBA1, markers for astrocytes and microglia, respectively. We found that APP/PS1 mice have significantly more reactive-like astrocytes and microglia in the cortex, as judged by positive immunostaining for GFAP and IBA1 than WT controls (Fig. 2 *A* and *B* and *SI Appendix*, Fig. S3 *A* and *B*). A previous study showed that global neuronal loss is not observed in APP/PS1 mice (29). Since NLRP3 is more specific to microglia, this may explain our results that NLRP3 increases at 12 mo. Astrocytes and microglia were activated in the cortex and hippocampus of AD mice, and this was normalized by treatment with NR (Fig. 2 *A* and *B* and *SI Appendix*, Fig. S3*C*). Together with the results from the microarray analyses, this suggests that NR reduces neuroinflammation in AD. Activation of astrocytes and microglia results in the release of proinflammatory cytokines and chemokines, which can cause damage to neurons (21). Thus, we investigated whether NR treatment changes proinflammatory cytokine and chemokine levels in AD mouse brains. Interferon gamma-inducible protein 10 (IP-10), RANTES, and MIP-1β were significantly elevated in AD cerebral cortex and reduced after NR treatment (Fig. 2 *C–E*). Similar to the brain, levels of proinflammatory cytokines and chemokines in the blood have also been reported to be higher in AD (30). In blood, the proinflammatory cytokine TNF-α was significantly increased in AD mice and decreased after NR treatment, and IL-1β trended toward an increase in AD mice and decreased significantly after NR treatment (Fig. 2 *F* and *G*). Keratinocyte-derived chemokine (CXCL1/KC), a potent chemoattractant for neutrophils expressed by astrocytes and microglia, also increased in AD mice blood and decreased significantly after NR treatment (*SI Appendix*, Fig. S3*D*). Interestingly, NR increased KC levels in WT mice blood, which suggests that NR may participate in regulating astrocytes and microglia in WT mice.

We next examined neuroinflammation-related protein expression in brains of AD mice. NR treatment reduced NLRP3 levels in the cerebral cortex of AD mice (Fig. 2*H* and *SI Appendix*, Fig. S3*E*). Caspase-1 and IL-1β levels were also normalized by NR in AD mouse brains, indicating that NR reduces the activity of the NLRP3 inflammasome (Fig. 2*H* and *SI Appendix*, Fig. S3 *F* and *G*). The NLRP3 inflammasome is activated by NF-κB (31), which in turn induces the release of downstream inflammatory factors. Thus, we investigated whether NR normalized the activity of NF-κB by measuring p65. The level of p65 was elevated in the brains of AD mice and restored in NR-treated AD mice (Fig. 2*H* and *SI Appendix*, Fig. S3*H*). Interferon gamma (IFN-γ) has antiviral, immunomodulatory, and antitumor properties (32). NR treatment decreased IFN-γ and IL-18 in AD mouse brains (*SI Appendix*, Fig. S3 *I* and *J*). Taken together, we found that NR suppresses the NLRP3 expression. For further validation, immunofluorescence of NLRP3 and Caspase-1 were significantly higher in the hippocampus and cortex of AD mice, compared to WT, and NR decreased their expression (Fig. 2 *I* and *J* and *SI Appendix*, Fig. S3*K*). The inflammatory response is also a biological response to DNA damage (33). Therefore, we evaluated DNA damage responses in brain tissue samples from NR-treated and control WT and AD mice. γ-H2AX is a marker for DNA damage while Cleaved-caspase-3 is a marker for apoptosis, and both showed a significant increase in the hippocampus and cortex of AD mouse brains. NR significantly reduced expression of these markers in the hippocampus and cortex of AD mouse brains (Fig. 2 *K* and *L* and *SI Appendix*, Fig. S3*L*). We also noted a slight increase in apoptosis in WT mice following NR treatment, $P = 0.057$, which is the opposite direction of what is expected from the treated AD mice (*SI Appendix*, Fig. S3*L*). These results suggest that NR decreases neuroinflammation and DNA damage in AD mouse brains; however, the underlying mechanisms are still unclear.

NR Attenuates Neuroinflammation through the cGAS–STING Pathway. Recent studies have shown that the cGAS and STING detect cytosolic DNA and are activated by DNA damage and neuroinflammation (19, 34). Since NR reduced DNA damage and neuroinflammation in AD mice, we speculated that this may occur via the cGAS–STING pathway. The expression of cGAS and STING proteins were quantified in the brains of AD and WT mice at different ages (3, 7, 12, and 20 mo). The levels of cGAS were higher in AD than WT mice at 7, 12, and 20 mo, and STING was significantly higher in AD than WT mice at 12 mo (Fig. 3 *A–C*). Note that the levels of cGAS and STING are different in different age groups, which may be due to the different levels of immune activation in WT and AD mice at different ages. Importantly, NR treatment significantly reduced expression of STING protein and trended to decrease cGAS expression in 12-mo AD mice (Fig. 3 *D–F*). Therefore, we speculated that NR may down-regulate neuroinflammation through the cGAS–STING pathway.

Because they are the main immune cells of the central nervous system, we used microglial cells for further studies. HMC3 human microglial cells were treated with $A\beta_{42}$ (5 μM) with or without NR for 48 h, and enzyme-linked immunosorbent assay (ELISA) results showed that IL-6 expression, in the cellular supernatant, was increased (Fig. 3*G*). IL-6 is a proinflammatory cytokine that induces the detrimental phenotype in microglia (8). However, when NR was administered with $A\beta_{42}$, IL-6 levels decreased (Fig. 3*G*). Treatment of microglial cells with the STING inhibitor H-151 completely prevented $A\beta_{42}$-induced IL-6 production, but NR did not decrease IL-6 in H-151–treated cells (Fig. 3*G*), suggesting that NR decreasing IL-6 is dependent upon STING. To directly confirm the role of cGAS–STING in Aβ-induced neuroinflammation, microglial cells were treated with small interfering RNA (siRNA): cGAS-siRNA and/or STING-siRNA, and with or without $A\beta_{42}$, and NR treatment. The cGAS or STING knockdown efficiencies are shown in *SI Appendix*, Fig. S4*A*. Consistent with the effect of the STING inhibitor, NR did not decrease IL-6 in the cGAS-knockdown and/or STING-knockdown microglial cells (Fig. 3*G*), suggesting that NR decreases IL-6 in a cGAS- and STING-dependent manner.

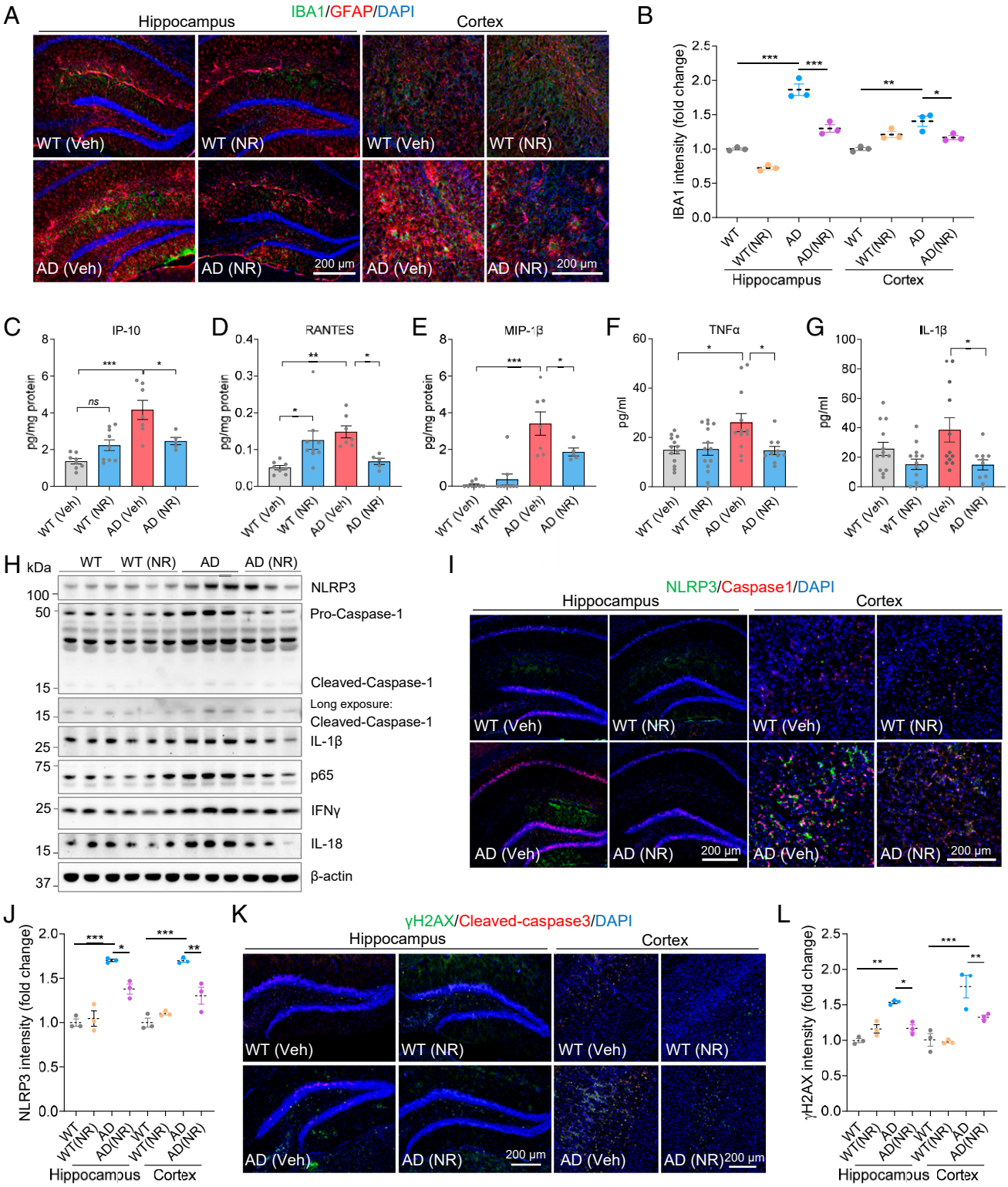

Fig. 2. NR decreases neuroinflammation, the NLRP3 inflammasome, NF-κB, and DNA damage. (*A*) Representative immunostaining images of IBA1 (green) and GFAP (red) with DAPI (blue) in mouse hippocampi and cortex. (*B*) Quantification of IBA1 intensity in *A*. $n = 3$ mice per group. (*C–E*) Proinflammatory cytokines or chemokines IP-10 (*C*), RANTES (*D*), and MIP-1β (*E*) levels detected by cytokine array in AD or WT mice cortex with or without NR treatment. $n = 5$ to 9 mice per group. (*F* and *G*) Proinflammatory cytokines or chemokines TNF-α (*F*) and IL-1β (*G*) levels detected by cytokine array in AD or WT mice plasma with or without NR treatment. $n = 10$ to 14 mice per group. (*H*) Western blots of specified proteins in WT and AD mice cortex with or without NR treatment. $n = 3$ mice per group. (*I*) Representative immunostaining images of NLRP3 (green) and caspase-1 (red) with DAPI (blue) in mice hippocampi and cortex. (*J*) Quantification of NLRP3 intensity in *I*. $n = 3$ mice per group. (*K*) Representative immunostaining images of γ-H2AX (green) and Cleaved-caspase-3 (red) with DAPI (blue) in mice hippocampi and cortex. (*L*) Quantification of γ-H2AX intensity in *K*. $n = 3$ mice per group. Data: mean ± SEM. Statistical significance was performed with two-way ANOVA followed by Tukey's or Bonferroni multiple comparisons test compared with control. $^*P < 0.05$, $^{**}P < 0.01$, $^{***}P < 0.001$.

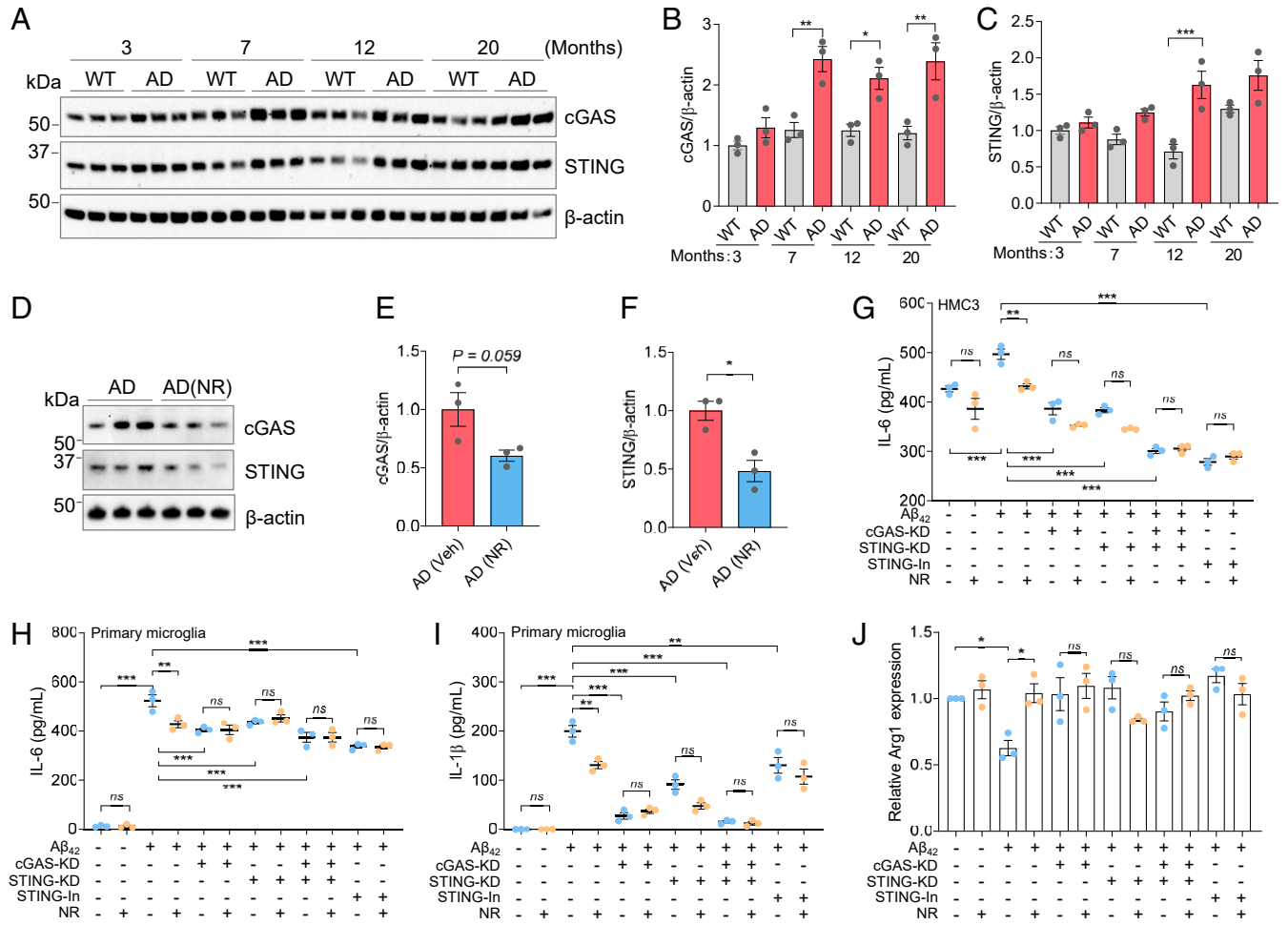

Fig. 3. NR attenuates neuroinflammation through the cGAS–STING pathway. (*A*) Western blots of specific proteins in different ages of AD and WT mice. n = 3 mice per group. (*B*) Quantification of cGAS protein level in *A*. (*C*) Quantification of STING protein level in *A*. (*D*) Western blots of specific proteins from 12-mo-old AD mice with/without NR treatment (12 mM, 5 mo). n = 3 mice per group. (*E*) Quantification of cGAS protein level in *D*. (*F*) Quantification of STING protein level in *D*. (*G*) ELISA of IL-6 level in different conditions of HMC3 cell supernatants. Cells were treated by combining $A\beta_{42}$ (5 μM) and/or NR (1 mM) and/or STING inhibitor or cGAS-KD and/or STING-KD for 48 h. n = 3 biological repeats. (*H*) ELISA of IL-6 level in different conditions of mouse primary microglia cell supernatants. Cells were treated by combining $A\beta_{42}$ (5 μM) and/or NR (1 mM) and/or STING inhibitor H151 (1 μM) or cGAS-KD and/or STING-KD for 72 h. n = 3 biological repeats. (*I*) ELISA of IL-1β level, same cell setting as *H*. (*J*) qPCR of M2 maker Arg1 in different conditions of mouse primary microglia cell, same cell setting as *H*. Data: mean ± SEM. Statistical significance was performed with Student's *t* test or one-way or two-way ANOVA followed by Tukey's multiple comparisons test. $^*P < 0.05$, $^{**}P < 0.01$, $^{***}P < 0.001$. Ns, not significant.

To validate the findings from human immortalized cells, we extended our approach by using mouse primary microglia. Primary microglial cells were treated with $A\beta_{42}$ (5 μM) with or without NR, or with siRNAs (cGAS-siRNA and/or STING-siRNA), or with STING inhibitor H-151 for 72 h. Knockdown efficiencies are shown in *SI Appendix*, Fig. S4 *B* and *C*. We found that the expression of the main proinflammatory markers IL-6, IL-1β, and TNF-α were increased in the $A\beta_{42}$-treated cell supernatant and decreased after NR treatment by ELISA (Fig. 3 *H* and *I* and *SI Appendix*, Fig. S4*D*). These effects were diminished when cGAS and/or STING was knocked down or inhibited (Fig. 3 *H* and *I* and *SI Appendix*, Fig. S4*D*). This confirms that NR decreases proinflammatory cytokines depending on cGAS/STING. In some of the tested conditions there was a trend toward decreased interleukins production, for example, in STING-knockdown (KD) conditions, NR has a trend to decrease IL-1β (Fig. 3*I*), which suggests that besides cGAS–STING, NR may be dependent on other mechanisms or pathways to decrease interleukin production. To further investigate whether NR plays a role in regulating anti-inflammatory markers, we examined the protective microglia markers Arg1 and Fizz1 using mouse primary microglia. Our results showed that the Arg1 levels were decreased in $A\beta_{42}$-treated primary microglia and that NR increased Arg1 and Fizz1 expression (Fig. 3*J* and *SI Appendix*, Fig. S4*E*). Similarly, we found that cGAS and STING are required to increase protective microglia state in response to NR treatment, since the effect of NR was diminished when cGAS/STING were knocked down or inhibited (Fig. 3*J* and *SI Appendix*, Fig. S4*E*). Combined, the data suggest that NR decreases neuroinflammation in microglia through reduced activation of the cGAS–STING pathway.

NR Decreases Cytoplasmic DNA by Inducing Mitophagy. cGAS–STING is a cytosolic DNA-sensing pathway. Cytoplasmic single-stranded DNA (ssDNA) or double-stranded DNA (dsDNA) activates STING to trigger downstream cellular responses (35). To investigate the level of cytoplasmic DNA in AD before and after NR treatment, we stained for dsDNA or ssDNA in NR- or vehicle-treated AD and WT mouse brain sections. While dsDNA appeared unchanged in AD compared to WT mouse brains, ssDNA was significantly higher in AD mouse brains compared to WT and NR decreased it significantly (Fig. 4 *A* and *C*). To test whether the results from mice

also apply to humans, we used human AD fibroblasts. Interestingly, both cytosolic ssDNA and dsDNA were significantly higher in human AD fibroblasts than in the corresponding control fibroblasts (Fig. 4 *B* and *D*). These results further confirm that cytoplasmic DNA is significantly up-regulated in AD human cells and mouse brains. We further investigated the nature of the increased cytoplasmic DNA and found that mitochondrial DNA (mtDNA) release was significantly increased in the cytoplasm (Fig. 4*E*) in human fibroblasts and that NR reduced cytoplasmic mtDNA levels (Fig. 4*E*) as measured per total mitochondria DNA. A recent study showed that a mitophagy deficiency promoted mtDNA release and activation of the cGAS–STING pathway in mouse heart tissue, which led to a strong inflammatory phenotype (34). Mitophagy has a major role in clearance of damaged and/or dysfunctional mitochondria, and we have documented compromised mitophagy in the brains of human AD patients and mouse models of AD (36). The level of mitophagy in NR-treated AD mouse brains was higher as monitored by the colocalization of mitochondrial protein TOMM20 and lysosomal protein LAMP2 (Fig. 4 *F* and *G*). To further validate the mitophagy findings, we analyzed some mitophagy-related markers. It has been shown that AMPK regulates energy expenditure and may be involved in mitophagy (37). Indeed, AMPK activity, as detected using antibodies specific for phosphorylated forms of AMPK (p-Thr127) were lower in AD mouse brains, and NR treatment increased the level of phosphorylated AMPK (Fig. 4*H* and *SI Appendix*, Fig. S4*F*). ULK1 is critical in mitophagy (38) and NR increased p-ULK1 (Fig. 4*H* and *SI Appendix*, Fig. S4*G*). LC3-II and p62/SQTMS1 have been shown to regulate mitophagy (39). NR decreased p62 levels and increased LC3-II (Fig. 4*H* and *SI Appendix*, Fig. S4 *H–J*). We also added the estimation statistics to the regular statistics for visualization (*SI Appendix*, Fig. S4 *F–J*, *Bottom* panels). These results suggest that NR induces mitophagy in AD mouse brains.

Our previous study on *Caenorhabditis elegans* model of AD found that NAD^+ precursor NMN induces mitophagy in a *pink1*-, *pdr1*-, *dct1*-dependent manner (36). Here, to investigate the molecular mechanisms by which NR induces mitophagy and whether induction of mitophagy plays a role in regulating cytoplasmic DNA, we depleted some key mitophagy-related genes in AD human fibroblasts (knockdown efficiencies are in *SI Appendix*, Fig. S4 *K–M*) and found that NR-induced mitophagy was dependent on the key mitophagy genes PINK1, ULK1, and NIX (Fig. 4*I* and *SI Appendix*, Fig. S5*A*). Cytosolic dsDNA was not decreased by NR treatment when PINK1, ULK1, or NIX were single knocked down, suggesting that mitophagy is required for NR to decrease cytoplasmic dsDNA in AD (Fig. 4 *J* and *L*). Interestingly, since cytoplasmic ssDNA was decreased by NR when PINK1 or ULK1 were knocked down, but not NIX, it suggests that NIX is specifically required for NR to decrease ssDNA (Fig. 4 *K* and *M*). We note that other pathways may also participate in the process. While we document mitophagy–gene dependent liberation of dsDNA and ssDNA, we cannot exclude the possibility that other mechanisms are involved.

These results indicate that NR increases mitophagy, thereby reducing mtDNA release to the cytosol, reduces other cytoplasmic DNAs, and reduces STING-dependent neuroinflammation.

NR Attenuates Cellular Senescence in AD. Several studies have provided strong evidence that genomic DNA damage leads to neuroinflammation, which can promote cellular senescence, and recent findings suggest that cell senescence occurs in glial cells in AD (40). In the present study, we found that AD mice, at 12 mo of age, have more SA-β-gal staining in their hippocampus and cortex than age-matched WT littermates. Interestingly, NR treatment decreased the SA-β-gal staining in the hippocampus and cortex of AD mice, relative to the vehicle controls (Fig. 5 *A* and *B*). To further confirm these results, we stained brain sections for the cellular senescence-related marker $p16^{INK4a}$ and found that the intensity of $p16^{INK4a}$ in the cortex of AD mice was significantly higher than that of WT mice. Notably, $p16^{INK4a}$ intensity was down-regulated in NR-treated AD mice (Fig. 5 *C* and *D*). Furthermore, senescence markers $p16^{INK4a}$, p21, and p15 have been reported to increase in age-related neurodegeneration, and we found that their mRNA levels were all elevated in the cortex of AD mice and decreased after NR treatment (Fig. 5 *E* and *F* and *SI Appendix*, Fig. S6*A*). As mentioned earlier, SASP is one of the main characteristics of senescence and includes the production of proinflammatory cytokines and chemokines. IP-10, RANTES, MIP-1β, TNF-α, and IL-1β, which are all proinflammatory, are decreased significantly after NR treatment (Fig. 2 *C–G*). This further confirms that NR can reduce cellular senescence in AD mice.

In order to investigate which cell types undergo senescence in the AD brain, we costained for the cellular senescence marker $p16^{INK4a}$ together with markers of different brain cells: microglia marker IBA1, astrocyte marker GFAP, neuron marker NeuN, and oligodendrocytes progenitor cell marker Olig2. Our results showed that microglia (Fig. 5*G*), astrocytes (Fig. 5*G*), neurons (Fig. 5*H*), and oligodendrocyte progenitor cells (Fig. 5*H*) had $p16^{INK4a}$ colocalization, indicating that all these cell types express this senescent cell marker. To confirm this, we used another senescence marker, p21, and costained with markers of the mentioned four brain makers and found that these four cell types (microglia, astrocytes, neurons, and oligodendrocyte progenitor cells) were positively stained for the senescent cell marker p21 (*SI Appendix*, Fig. S6*B*). Combined, the data support the role of senescence in AD and suggest that NAD^+ augmentation has anti-senescence and/or senolytic effects.

As mentioned before, previous studies have shown that DNA damage can cause cellular senescence (19). To investigate the relationship between DNA damage and senescence in AD brains, we stained for DNA damage marker γ-H2AX and the senescence marker p21 in APP/PS1 mouse brain sections. The results showed that γ-H2AX and p21 colocalized in AD mouse brains (*SI Appendix*, Fig. S6*C*), which indicates that cellular senescence in AD mouse brains is associated with DNA damage.

NR Decreases Senescence in HMC3 Cells through the cGAS–STING Pathway. To elucidate the mechanism by which NR affects glial senescence, we treated HMC3 microglial cells with etoposide to induce senescence. Etoposide is a topoisomerase inhibitor and a cytotoxic anticancer agent, which induces DNA damage and cellular senescence (20). NR (1 mM) decreased etoposide-induced senescence (SA-β-gal) in the HMC3 microglial cells (Fig. 5 *I* and *J*). The innate cGAS–STING DNA-sensing pathway regulates senescence by recognizing cytosolic DNA and inducing SASP factors (20, 41). cGAS is essential for cellular senescence, including the expression of inflammatory genes (20). A previous study has reported that modulation of cGAS activity may be a new strategy to treat senescence-associated human diseases (20). To investigate whether NR works through the cGAS–STING pathway, we depleted cGAS, STING, or used a STING inhibitor in HMC3 microglial cells. Although the SA-β-gal signal was lower after cGAS or STING knockdown, the remaining SA-β-gal staining could not be further reduced by NR treatment in cGAS or STING-deficient cells (Fig. 5 *I* and *J*), thus indicating that the effect of NR is dependent upon cGAS–STING signaling. Another way to induce senescence is by irradiation. Consistent with the results of the etoposide-treated cells, NR decreased senescence in IR-treated (3 Gy, followed by 9 d in culture) HMC3 cells but not in cGAS or STING knockdown HMC3 cells (*SI Appendix*, Fig. S6 *D* and *E*). These results further support that NR decreases senescence in HMC3 cells through the cGAS–STING pathway.

NR Promotes the Protective Microglial Phenotype, Improving Microglial Phagocytosis of Aβ. Microglia play multifaceted roles in neurological diseases. Detrimental "inflammatory" state microglia produce proinflammatory cytokines, which are detrimental to neurons, while

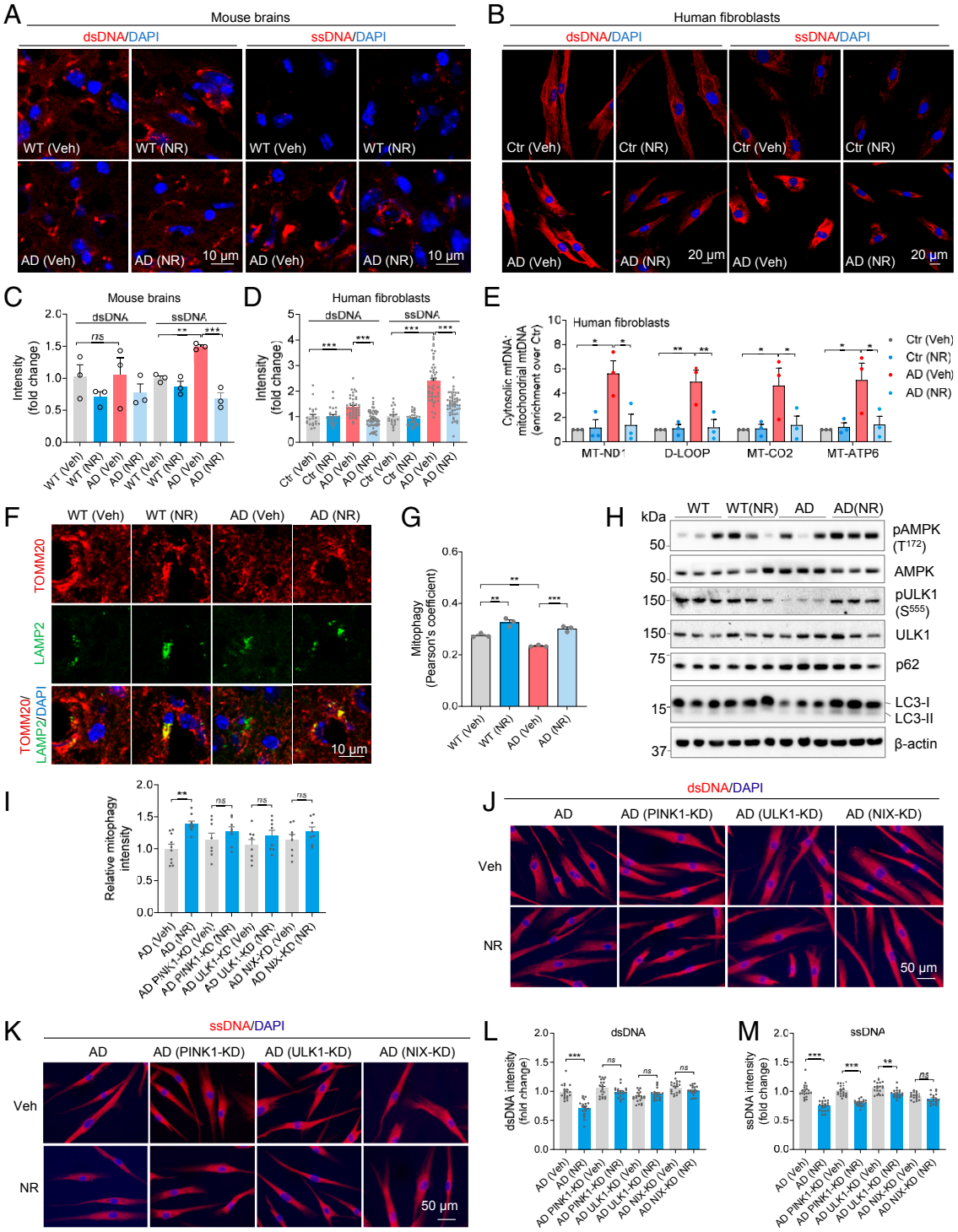

Fig. 4. NR decreases cGAS–STING by decreasing cytoplasmic DNA. (*A*) Immunostaining of dsDNA and ssDNA with DAPI in mouse brain sections. $n = 3$ mice per group. (*B*) Immunostaining of dsDNA and ssDNA with DAPI in AD human fibroblasts and control fibroblasts. $n = 21$ to 58 cells per group were analyzed. (*C*) Quantification of dsDNA and ssDNA in *A*. $n = 3$ mice per group. (*D*) Quantification of dsDNA and ssDNA in *B*. (*E*) Total DNA was harvested from cytosolic and mitochondrial fractions of human fibroblasts and analyzed by qPCR. Cytosolic mtDNA genes were normalized to respective mitochondrial mtDNA genes (mt-ND1, D-loop, MT-CO_2, MT-ATP6) and presented as fold enrichment over vehicle-treated controls (*Methods*). $n = 3$ biological repeats. (*F*) Immunostaining of TOMM20 and LAMP2 with DAPI in mouse brain sections. (*G*) Quantification of mitophagy (colocalization of TOMM20 and LAMP2) in *F*. $n = 3$ mice per group. (*H*) Western blots of specific proteins in NR- or vehicle-treated AD and WT mice brain cortex. $n = 3$ mice per group. (*I*) Relative mitophagy intensity in AD human fibroblasts after some key mitophagy genes knockdown. Quantification of mitophagy in *SI Appendix*, Fig. S5*A*. $n = 8$ to 10 images per group were analyzed. (*J*) Immunostaining of dsDNA with DAPI in AD human fibroblasts after some mitophagy genes knockdown. (*K*) Immunostaining of ssDNA with DAPI in AD human fibroblasts after some mitophagy genes knockdown. (*L* and *M*) Quantification of dsDNA and ssDNA in *J* and *K*. $n = 20$ cells per group were analyzed. Data: mean ± SEM. Statistical significance was performed with two-way ANOVA followed by Tukey's multiple comparisons test. $^*P < 0.05$, $^{**}P < 0.01$, $^{***}P < 0.001$. Ns, not significant.

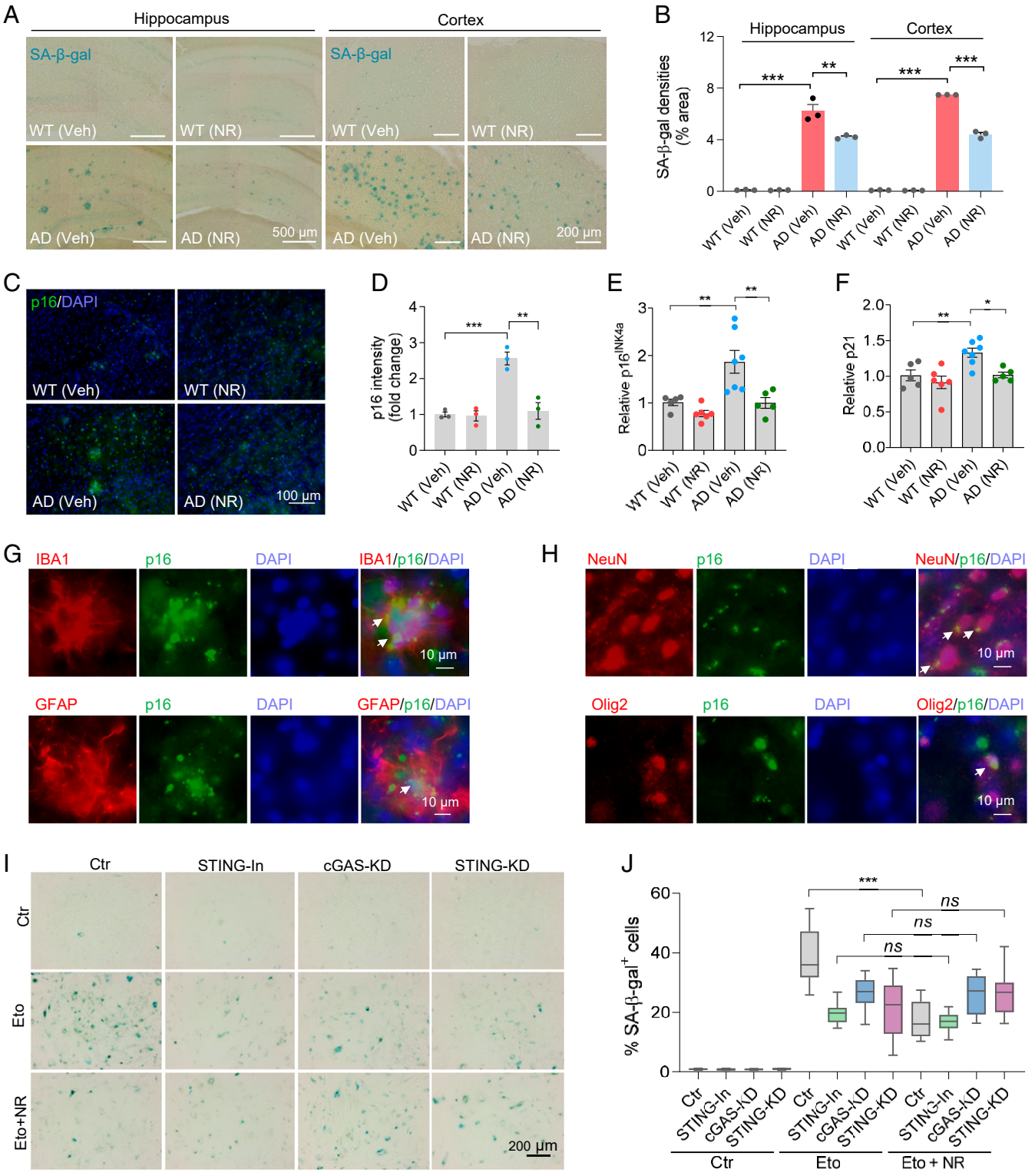

Fig. 5. NR decreases cellular senescence in AD mouse brains. (*A*) Representative SA-β-gal staining in NR- or vehicle-treated AD or WT mice hippocampi and cortex. The panels of the hippocampus are part of the pictures after stitching the entire hippocampus with mosaic tile scan of microscope, and some of the stitching areas are still visible. (*B*) Quantification of SA-β-gal staining densities in *A*. $n = 3$ mice per group. (*C*) Representative $p16^{INK4a}$ staining in NR- or vehicle-treated AD or WT mouse brains. (*D*) Quantification of $p16^{INK4a}$ staining intensity in *C*. $n = 3$ mice per group. (*E* and *F*) Real-time qPCR of relative $p16^{INK4a}$ and p21 mRNA levels. $n = 5$ to 7 mice per group. (*G*) Immunofluorescence of microglia marker IBA1 (red) or astrocyte marker GFAP (red) with cellular senescence marker $p16^{INK4a}$ (green) in AD mouse brains. White arrows point to colocalization. (*H*) Immunofluorescence of neuron marker NeuN (red) or oligodendrocyte progenitor cell marker Olig2 (red) with cellular senescence marker $p16^{INK4a}$ (green) in AD mouse brains. White arrows point to colocalization. (*I*) Representative SA-β-gal staining in etoposide- (Eto, 3 μM for 24 h and then washed the cells with fresh medium and incubated them an additional 4 d) or vehicle-treated HMC3 microglia cells. Cells were treated with STING inhibitor, or cGAS siRNA, or STING siRNA. (*J*) Quantification of SA-β-gal positive cells in *I*. $n = 18$ pictures per group. Data: mean ± SEM. Statistical significance was performed with two-way ANOVA followed by Tukey's multiple comparisons test. $^*P < 0.05$, $^{**}P < 0.01$, $^{***}P < 0.001$. Ns, not significant.

protective homeostatic state microglia promote phagocytosis of Aβ and support neuronal viability and health (6, 7). To test the microglial cell state in NR-treated AD mouse brains, we performed immunostaining of Aβ (6E10 antibody) and microglia (IBA1 antibody). We found increased engulfment of Aβ by microglia after NR treatment (Fig. 6 *A* and *B*). Furthermore, in the brains of NR-treated animals, the microglial processes became shorter, showing that the phagocytic state of microglia had changed (*SI Appendix*, Fig. S6*F*). Consistent with this, NR increased the expression level of CSF2RA, a proliferation marker of microglia, without changing the expression level of osteopontin, a prominent component of the mineralized extracellular matrices of bones and teeth (Fig. 6 *C* and *D*). Microglia in NR-treated brains undergo an alternative protective state as characterized by increased expression of the markers Arg1, Fizz1, and YM1 (Fig. 6*E*). Combined, the results suggest that NR promotes a protective phenotype.

NR Improves Learning and Memory and Synaptic Plasticity in AD Mice. To investigate the effect of NR on behavior in APP/PS1 mice, performance in the Morris water maze and Y-maze tests were measured. In the Morris water maze training phase, APP/PS1 mice spent more time finding the hidden platform, while NR-treated APP/PS1 mice required less time to find the platform, showing that NR improves learning in APP/PS1 mice (Fig. 6*F* and *SI Appendix*, Fig. S7*A*). In the probe trial, when the platform was removed, AD mice spent less time in the target quadrant where the platform used to be and crossed the platform location less frequently, suggesting that the AD mice had memory deficiency (Fig. 6 *G* and *H*). NR increased the search time in the target quadrant and the frequency of crossing the platform location and decreased the latency to the platform location without influencing the swimming speed, indicating that NR improves memory ability in AD mice (Fig. 6 *G* and *H* and *SI Appendix*, Fig. S7 *B* and *C*). NR improved spatial working memory in another cognitive test (Y-maze test), which further confirmed that NR improves memory in APP/PS1 mice (*SI Appendix*, Fig. S7*D*). NR did not change the behaviors in the rotarod or grip strength test, suggesting that it did not affect motor function or muscle strength in 12-mo-old APP/PS1 mice (*SI Appendix*, Fig. S7 *E* and *F*). AD mice traveled more in the open field test, but the time in the center zone was the same as WT mice, suggesting that AD mice did not have increased anxiety (*SI Appendix*, Fig. S7 *G* and *H*). Because hippocampal neuronal circuits are widely considered as one of the major cellular mechanisms that underlies learning and memory, we performed electrophysiological recordings from CA1 neurons to measure long-term potentiation (LTP) at CA3–CA1 synapses. Field excitatory postsynaptic potentials were recorded in stratum radiatum of the CA1 region of the hippocampus in brain slices from WT and AD mice that had been maintained for 5 mo with or without NR treatment. There were no significant differences in basal synaptic transmission among the four groups of mice as indicated by identical input–output curves (*SI Appendix*, Fig. S7 *I* and *J*). However, LTP was significantly reduced in slices from AD mice compared to WT mice, and slices from NR-treated mice exhibited a significant increase in LTP, especially in the AD mice (40% increase), indicating that NR improves synaptic plasticity, consistent with the results of learning and memory (Fig. 6 *I* and *J*).

Discussion

Neuroinflammation and senescence occur in AD; however, the mechanism is still unclear. Here, we found that neuroinflammation and senescence may be mediated by cGAS–STING pathway. Furthermore, treatment with NR decreased neuroinflammation and cellular senescence in the brains of AD mice via inhibition of cGAS–STING signaling. NR also decreased the NLRP3 inflammasome, DNA damage, and increased microglial phagocytosis of Aβ.

Senescent cells accumulate during normal aging and AD, and their SASP is believed to contribute to age-related tissue inflammation (42). Previous studies report that the cGAS–STING pathway affects neuroinflammation, DNA damage, and senescence (19) and that neuroinflammation may drive the progression of AD. Investigating how the cytosolic DNA-sensing pathway cGAS–STING is activated in AD, we found that cytosolic DNAs were increased in AD mice and AD human fibroblasts. AD cells had a significant three- to sixfold enrichment of mtDNA in the cytosolic fraction per mitochondrial fraction compared to WT cells, suggesting that damaged mitochondria released mtDNA to cytosol in AD. Studies have reported alternative ways by which mtDNA can be released into the cytosol, which include TFAM deficiency (43) or activation of the pro-death proteins BAK and BAX (44). Of note, we showed that NR decreased cytoplasmic DNA in AD via induction of mitophagy. We propose that due to the mitophagy deficiency in the AD samples, more DNA is released into the cytosol, which causes increased activation of cGAS–STING, leading to abnormal neuroinflammation and cellular senescence.

We confirmed compromised mitophagy in AD in this study, an extension of our previous results (36). NAD^+ modulates mitochondrial homeostasis, which plays major roles in mitochondrial metabolism, neuroprotection, and aging. Supplementation with compounds that increase the endogenous pool of NAD^+ (for example, NR and NMN) may improve lifespan and healthspan and delay the onset or ameliorate pathological features of some age-related diseases, including AD, Parkinson's disease (PD), amyotrophic lateral sclerosis, and ataxia telangiectasia (13, 14, 45) via mitophagy. Here, we showed that NR-induced mitophagy in the APP/PS1 mouse model, and NR treatment leads to reduced DNA release into the cytosol, thereby reducing the abnormal activation of the DNA-sensing pathway, leading to a normalization of neuroinflammation and less senescence in the AD brain. One recent study on PD found that PINK or Parkin knock-out mice accumulate mutations in mtDNA and display inflammation, which can be rescued by concurrent loss of STING (34). Our current study supports a role for PINK1- and PARKIN-mediated mitophagy in restraining innate immunity. Recent studies indicate that accumulation of cytoplasmic DNA and STING pathway activation contribute to inflammatory responses in Huntington's disease, traumatic brain injury, and ataxia telangiectasia (46–49). Our current study links the cGAS–STING pathway to AD. We found that NAD^+ induced mitophagy, inhibited the cGAS–STING pathway, and our experiments with human microglial cells suggest that the cGAS–STING plays a crucial role in reducing neuroinflammation and senescence in AD. Whether other mitophagy inducers (such as Urolithin A) have the same effect remains to be investigated.

The anti-inflammatory effects of NR are also supported by other studies. Oral NR supplementation in aged human participants augments the skeletal muscle NAD^+ metabolome and induces anti-inflammatory signatures (50); NR, NMN, and other NAD^+ precursors also reduce inflammation in animal models of ataxia telangiectasia (51). Though chronic inflammation is a hallmark feature of aging and AD, use of NR may also find utility in other chronic inflammatory disorders. We found that there is a significant difference in NAD^+/NADH at 7 mo, between AD and WT, which may not impact NLRP3, as there are many other factors and molecular mechanisms that may be involved. There is a slight upward trend of apoptosis in WT after NR treatment. A limitation of our analysis of protein lysates is that it did not include an analysis of cell type ratio. Future work should address which cell types in WT brains may have apoptotic changes after NR treatment.

Some studies have reported senescent astrocytes, microglia, and oligodendrocyte progenitors in AD brains (5, 11, 12). Recently, NAD^+ has been shown to rescue D-galactose–induced cellular senescence in cardiomyocytes (52). However, another study found that NAD^+ metabolism governs the proinflammatory SASP in cancer (53). Here, we show increased cellular senescence in AD, and increasing NAD^+ levels may decrease this senescence. We also found senescent microglia, astrocytes, neurons, and oligodendrocyte

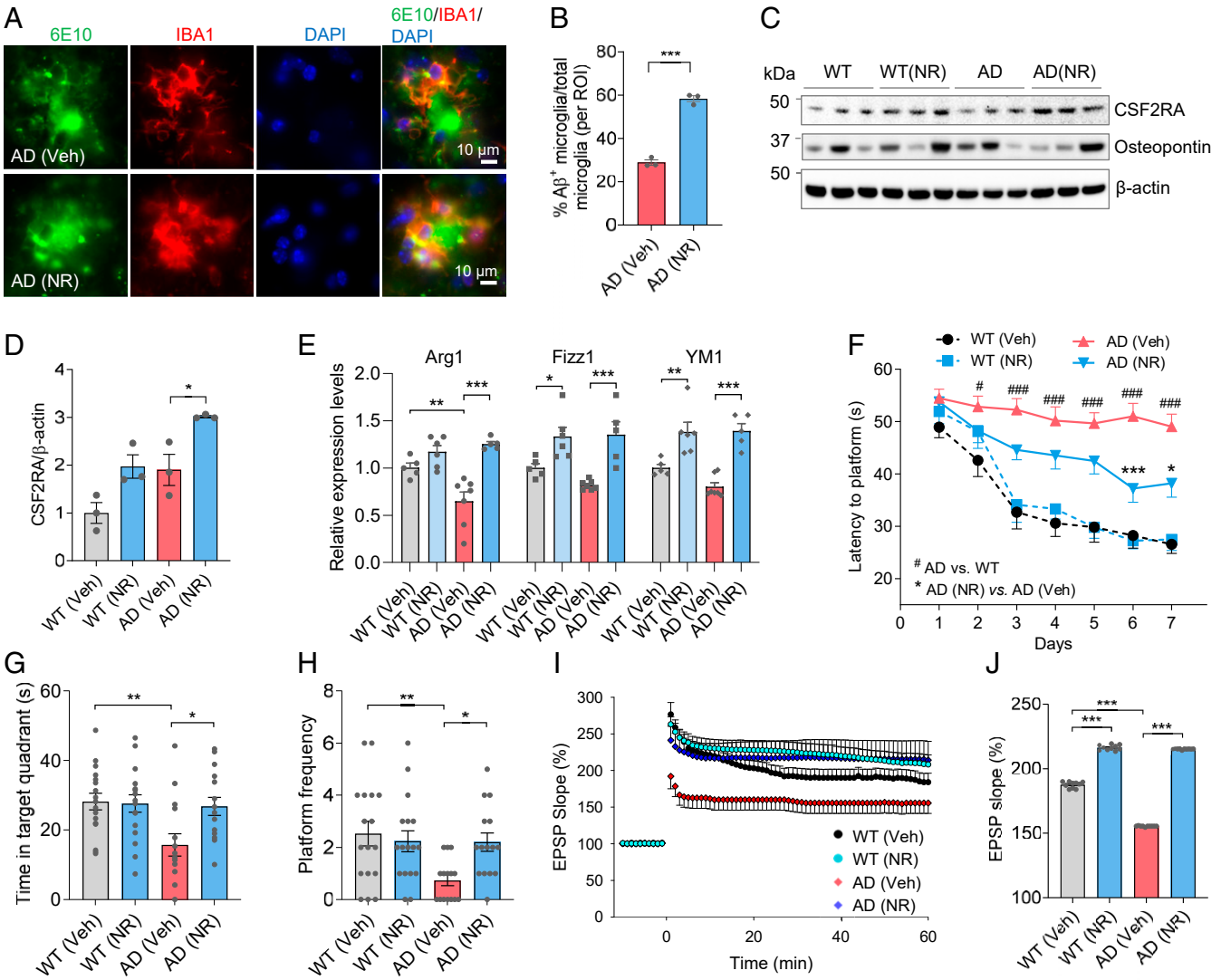

Fig. 6. NR promotes a protective microglial phenotype and improves cognition and LTP in AD mice. (*A*) Representative immunostaining colocalization of Aβ (6E10) and microglia (IBA1) in NR- or vehicle-treated AD mouse brains. (*B*) Quantification of Aβ-positive microglia per region of interest (ROI) in NR- or vehicle-treated NR mouse brains (related to *A*). $n = 3$ mice per group. (*C*) Western blots of specific proteins in NR- or vehicle-treated AD and WT mice brain cortex. $n = 3$ mice per group. (*D*) Quantification of CSF2RA protein levels in *C*. (*E*) Real-time qPCR of protective microglia markers Arg1, Fizz1, and YM1 in AD or WT mice brain cortex with or without NR treatment. $n = 5$ to 7 mice per group. (*F*) Training phase of the Morris water maze test. The latency to find the platform was shown in NR- or vehicle-treated AD and WT mice. $n = 15$ to 17 mice per group. # comparison between AD versus WT. $^{\#}P < 0.05$. $^{\#\#\#}P < 0.001$. * comparison between NR-treated AD versus vehicle-treated AD. $^{*}P < 0.05$, $^{***}P < 0.001$. (*G*) Time in the target quadrant of mice in the probe trial of Morris water maze. (*H*) Frequency to cross the location of the platform of mice in the probe trial of Morris water maze. $n = 15$ to 17 mice per group. (*I*) The LTP in mice hippocampus CA1. $n = 5$ mice per group. (*J*) Quantification of 50 to 60 min LTP magnitude in mice hippocampus CA1. Data: mean ± SEM. Statistical significance was performed with Student's *t* test for two groups or two-way ANOVA followed by Tukey's multiple comparisons test. $^{*}P < 0.05$, $^{**}P < 0.01$, $^{***}P < 0.001$.

progenitor cells in the AD mouse brains. All these cell types have been reported to be senescent in AD in previous studies, and we have here validated senescence in these cell types in this current study (11, 12, 54–56).

Microglia and astrocyte activation in the AD brain release inflammatory cytokines, promoting neurodegeneration. Moreover, microglia lost their phagocytosis of Aβ function in AD mice and exhibit a detrimental microglial phenotype, while NR made the microglia transition from the detrimental to protective phenotype.

It is worth noting that besides regulating cell senescence and inflammation through mitophagy, NR may also bring benefits to AD mice through other mechanisms. DNA damage is closely related to cell senescence and inflammation. We had previously reported that NR improves nonhomologous end joining–mediated double-strand break repair by up-regulating NAD^+/SIRT1 signaling (51). NAD^+-dependent SIRT1 participates in DNA repair by activating ATM and Ku70 (57). Other NAD-dependent sirtuin members, including SIRT6 and SIRT3, may also help to improve DNA repair through NAD^+ supplementation. NR also can reduce ROS production and improve other mitochondrial functions in addition to mitophagy (51, 58).

NAD^+ precursors, such as NR, are dietary supplements and generally considered safe and have already been tested on healthy individuals, even at high doses, with no toxic side effects observed (59). There are several ongoing clinical trials using NR as a potential drug. The data suggest that NR is safe with no or minimal adverse effects (60).

Our results indicate that NR treatment may have different effects on WT and APP/PS1 mice. We found that NR reduced apoptosis and the levels of RANTES and KC in AD mice, while it increased

apoptosis and the levels of these proteins in WT mice (Fig. 2*D* and *SI Appendix*, Fig. S3 *D* and *L*). It may be caused by the difference in the basic NAD^+ levels between WT and AD mice. Furthermore, there may be age or localized drug effects on specific tissue. In our experiment, we used 7-mo-old mice and treated them with NR for 5 mo. Since WT mice are healthy, we found that their NAD^+ did not decrease significantly (Fig. 1*E*). In this case, further supplementation of NAD^+ may disturb the balance of NAD^+ metabolome and produce some unexpected effects. In addition, we only examined the hippocampus and cortical areas of the brain in the study, so we are not sure whether supplementation with NR will cause similar effects in other tissues in WT mice. For AD mice, compared with WT mice, the NAD^+/NADH ratio was significantly reduced in the previous report (14) and our current data (Fig. 1*G*). Since NAD^+ plays important roles in DNA repair and mitochondrial function, supplementing NAD^+ is vital and beneficial when NAD^+ levels are low (such as AD). Whether NAD^+ supplements are suitable for healthy people needs further research.

The study presented here provides insights into the interconnected network between NR, senescence, and neuroinflammation in AD and suggests potential targets for future interventional studies.

Methods

Mice. All animal experiments were performed and approved by the National Institute on Aging (NIA) Animal Care and Use Committee. All animals were maintained under standard conditions at the National Institute on Aging. The APP/PS1 mouse strain (stock no. 004462 in Jackson's laboratory) is a widely used animal model for AD and has many features of human AD, including inflammation and synaptic plasticity. APP/PS1 and their littermates (WT) were used in this study. APP/PS1 and WT mice were treated with or without NR (12 mM, ChromaDex) in drinking water from 7 to 12 mo of age. The NR treatment was performed the same as our previous report (14). From 9 mo old, the mice were subsequently evaluated for a series of behavioral experiments.

Statistical Analysis. GraphPad Prism 6.0 was used for statistical analysis. Data shown is mean ± SEM with $P < 0.05$ considered statistically significant. Two-tailed unpaired *t* test was applied for comparisons between two groups. Group differences were analyzed with one-way or two-way ANOVA followed by Tukey's or Bonferroni multiple comparisons test for multiple groups. The estimation statistics and graphs were generated using tools on the website made by Adam Claridge-Chang and Joses Ho (https://www.estimationstats.com/#/) (61). The mean difference for two comparisons were shown in the Cumming estimation plot. The raw data were plotted on the upper axes; each mean difference was plotted on the lower axes as a bootstrap sampling distribution. Mean differences were depicted as dots; 95% CIs were indicated by the ends of the vertical error bars.

Details of mouse behavior tests, NAD^+ detection, microarray, electrophysiology, immunofluorescence, Western blots, cell culture, ELISA for cytokines, preparation of Aβ peptides, cytokine array, SA-β-gal staining, RNA extraction and real-time qPCR, and subcellular fractionation are provided in *SI Appendix*.

Data Availability. Microarray data have been deposited in Gene Expression Omnibus (GEO, accession number GSE135999). All other study data are included in the article and/or *SI Appendix*.

ACKNOWLEDGMENTS. This research was supported by the Intramural Research Program of the NIH, the National Institute on Aging (V.A.B.). We thank Drs. Yongqing Zhang, Elin Lehrmann, and Kevin Becker for performing microarray experiments and data analysis. We thank Drs. Xiuli Dan, Jaehyeon Park, and Louise Christiansen for critically reading the paper.

1. G. S. Bloom, Amyloid-β and tau: The trigger and bullet in Alzheimer disease pathogenesis. *JAMA Neurol.* **71**, 505–508 (2014).
2. M. G. Spillantini, M. Goedert, Tau pathology and neurodegeneration. *Lancet Neurol.* **12**, 609–622 (2013).
3. W. Y. Fu, X. Wang, N. Y. Ip, Targeting neuroinflammation as a therapeutic strategy for Alzheimer's disease: Mechanisms, drug candidates, and new opportunities. *ACS Chem. Neurosci.* **10**, 872–879 (2019).
4. A. Johri, M. F. Beal, Mitochondrial dysfunction in neurodegenerative diseases. *J. Pharmacol. Exp. Ther.* **342**, 619–630 (2012).
5. T. J. Bussian *et al*., Clearance of senescent glial cells prevents tau-dependent pathology and cognitive decline. *Nature* **562**, 578–582 (2018).
6. M. T. Heneka *et al*., Neuroinflammation in Alzheimer's disease. *Lancet Neurol.* **14**, 388–405 (2015).
7. F. Leng, P. Edison, Neuroinflammation and microglial activation in Alzheimer disease: Where do we go from here? *Nat. Rev. Neurol.* **17**, 157–172 (2021).
8. V. Calsolaro, P. Edison, Neuroinflammation in Alzheimer's disease: Current evidence and future directions. *Alzheimers Dement.* **12**, 719–732 (2016).
9. A. Lasry, Y. Ben-Neriah, Senescence-associated inflammatory responses: Aging and cancer perspectives. *Trends Immunol.* **36**, 217–228 (2015).
10. J. Campisi, Aging, cellular senescence, and cancer. *Annu. Rev. Physiol.* **75**, 685–705 (2013).
11. P. Zhang *et al*., Senolytic therapy alleviates Aβ-associated oligodendrocyte progenitor cell senescence and cognitive deficits in an Alzheimer's disease model. *Nat. Neurosci.* **22**, 719–728 (2019).
12. R. Bhat *et al*., Astrocyte senescence as a component of Alzheimer's disease. *PLoS One* **7**, e45069 (2012).
13. E. F. Fang *et al*., NAD^+ in aging: Molecular mechanisms and translational implications. *Trends Mol. Med.* **23**, 899–916 (2017).
14. Y. Hou *et al*., NAD^+ supplementation normalizes key Alzheimer's features and DNA damage responses in a new AD mouse model with introduced DNA repair deficiency. *Proc. Natl. Acad. Sci. U.S.A.* **115**, E1876–E1885 (2018).
15. K. F. Mills *et al*., Long-term administration of nicotinamide mononucleotide mitigates age-associated physiological decline in mice. *Cell Metab.* **24**, 795–806 (2016).
16. D. Ryu *et al*., NAD+ repletion improves muscle function in muscular dystrophy and counters global PARylation. *Sci. Transl. Med.* **8**, 361ra139 (2016).
17. A. Ablasser, Z. J. Chen, cGAS in action: Expanding roles in immunity and inflammation. *Science* **363**, eaat8657 (2019).
18. Q. Chen, L. Sun, Z. J. Chen, Regulation and function of the cGAS-STING pathway of cytosolic DNA sensing. *Nat. Immunol.* **17**, 1142–1149 (2016).
19. T. Li, Z. J. Chen, The cGAS-cGAMP-STING pathway connects DNA damage to inflammation, senescence, and cancer. *J. Exp. Med.* **215**, 1287–1299 (2018).
20. H. Yang, H. Wang, J. Ren, Q. Chen, Z. J. Chen, cGAS is essential for cellular senescence. *Proc. Natl. Acad. Sci. U.S.A.* **114**, E4612–E4620 (2017).
21. D. V. Hansen, J. E. Hanson, M. Sheng, Microglia in Alzheimer's disease. *J. Cell Biol.* **217**, 459–472 (2018).
22. M. S. Tan, J. T. Yu, T. Jiang, X. C. Zhu, L. Tan, The NLRP3 inflammasome in Alzheimer's disease. *Mol. Neurobiol.* **48**, 875–882 (2013).
23. M. T. Heneka *et al*., NLRP3 is activated in Alzheimer's disease and contributes to pathology in APP/PS1 mice. *Nature* **493**, 674–678 (2013).
24. C. Ising *et al*., NLRP3 inflammasome activation drives tau pathology. *Nature* **575**, 669–673 (2019).
25. D. Choubey, Type I interferon (IFN)-inducible absent in melanoma 2 proteins in neuroinflammation: Implications for Alzheimer's disease. *J. Neuroinflammation* **16**, 236 (2019).
26. D. Cheng, W. Logge, J. K. Low, B. Garner, T. Karl, Novel behavioural characteristics of the APP(Swe)/PS1ΔE9 transgenic mouse model of Alzheimer's disease. *Behav. Brain Res.* **245**, 120–127 (2013).
27. D. Cao, H. Lu, T. L. Lewis, L. Li, Intake of sucrose-sweetened water induces insulin resistance and exacerbates memory deficits and amyloidosis in a transgenic mouse model of Alzheimer disease. *J. Biol. Chem.* **282**, 36275–36282 (2007).
28. J. L. Jankowsky *et al*., Co-expression of multiple transgenes in mouse CNS: A comparison of strategies. *Biomol. Eng.* **17**, 157–165 (2001).
29. N. J. Rupp, B. M. Wegenast-Braun, R. Radde, M. E. Calhoun, M. Jucker, Early onset amyloid lesions lead to severe neuritic abnormalities and local, but not global neuron loss in APPPS1 transgenic mice. *Neurobiol. Aging* **32**, 2324.e2321–2326 (2011).
30. H. M. Snyder *et al*., Developing novel blood-based biomarkers for Alzheimer's disease. *Alzheimers Dement.* **10**, 109–114 (2014).
31. Z. Zhong *et al*., NF-κB restricts inflammasome activation via elimination of damaged mitochondria. *Cell* **164**, 896–910 (2016).
32. K. Schroder, P. J. Hertzog, T. Ravasi, D. A. Hume, Interferon-gamma: An overview of signals, mechanisms and functions. *J. Leukoc. Biol.* **75**, 163–189 (2004).
33. S. P. Jackson, J. Bartek, The DNA-damage response in human biology and disease. *Nature* **461**, 1071–1078 (2009).
34. D. A. Sliter *et al*., Parkin and PINK1 mitigate STING-induced inflammation. *Nature* **561**, 258–262 (2018).
35. T. Abe *et al*., STING recognition of cytoplasmic DNA instigates cellular defense. *Mol. Cell* **50**, 5–15 (2013).
36. E. F. Fang *et al*., Mitophagy inhibits amyloid-β and tau pathology and reverses cognitive deficits in models of Alzheimer's disease. *Nat. Neurosci.* **22**, 401–412 (2019).
37. D. F. Egan *et al*., Phosphorylation of ULK1 (hATG1) by AMP-activated protein kinase connects energy sensing to mitophagy. *Science* **331**, 456–461 (2011).
38. W. Wu *et al*., ULK1 translocates to mitochondria and phosphorylates FUNDC1 to regulate mitophagy. *EMBO Rep.* **15**, 566–575 (2014).
39. S. Geisler *et al*., PINK1/Parkin-mediated mitophagy is dependent on VDAC1 and p62/SQSTM1. *Nat. Cell Biol.* **12**, 119–131 (2010).
40. M. Kritsilis *et al*., Ageing, cellular senescence and neurodegenerative disease. *Int. J. Mol. Sci.* **19**, 2937 (2018).
41. M. Ruiz de Galarreta, A. Lujambio, DNA sensing in senescence. *Nat. Cell Biol.* **19**, 1008–1009 (2017).
42. D. J. Baker, R. C. Petersen, Cellular senescence in brain aging and neurodegenerative diseases: Evidence and perspectives. *J. Clin. Invest.* **128**, 1208–1216 (2018).

43. A. P. West *et al*., Mitochondrial DNA stress primes the antiviral innate immune response. *Nature* **520**, 553–557 (2015).
44. K. McArthur *et al*., BAK/BAX macropores facilitate mitochondrial herniation and mtDNA efflux during apoptosis. *Science* **359**, eaao6047 (2018).
45. H. Zhang *et al*., NAD^+ repletion improves mitochondrial and stem cell function and enhances life span in mice. *Science* **352**, 1436–1443 (2016).
46. X. Song, F. Ma, K. Herrup, Accumulation of cytoplasmic DNA due to ATM deficiency activates the microglial viral response system with neurotoxic consequences. *J. Neurosci.* **39**, 6378–6394 (2019).
47. A. Abdullah *et al*., STING-mediated type-I interferons contribute to the neuroinflammatory process and detrimental effects following traumatic brain injury. *J. Neuroinflammation* **15**, 323 (2018).
48. M. Sharma, S. Rajendrarao, N. Shahani, U. N. Ramírez-Jarquín, S. Subramaniam, Cyclic GMP-AMP synthase promotes the inflammatory and autophagy responses in Huntington disease. *Proc. Natl. Acad. Sci. U.S.A.* **117**, 15989–15999 (2020).
49. H. Quek *et al*., A rat model of ataxia-telangiectasia: Evidence for a neurodegenerative phenotype. *Hum. Mol. Genet.* **26**, 109–123 (2017).
50. Y. S. Elhassan *et al*., Nicotinamide riboside augments the aged human skeletal muscle NAD(+) metabolome and induces transcriptomic and anti-inflammatory signatures. *Cell Rep.* **28**, 1717–1728.e1716 (2019).
51. E. F. Fang *et al*., NAD^+ replenishment improves lifespan and healthspan in ataxia telangiectasia models via mitophagy and DNA repair. *Cell Metab.* **24**, 566–581 (2016).
52. L. F. Wang *et al*., CD38 deficiency alleviates D-galactose-induced myocardial cell senescence through NAD^+/Sirt1 signaling pathway. *Front. Physiol.* **10**, 1125 (2019).
53. T. Nacarelli *et al*., NAD^+ metabolism governs the proinflammatory senescence-associated secretome. *Nat. Cell Biol.* **21**, 397–407 (2019).
54. B. E. Flanary, N. W. Sammons, C. Nguyen, D. Walker, W. J. Streit, Evidence that aging and amyloid promote microglial cell senescence. *Rejuvenation Res.* **10**, 61–74 (2007).
55. X. Han, T. Zhang, H. Liu, Y. Mi, X. Gou, Astrocyte senescence and Alzheimer's disease: A review. *Front. Aging Neurosci.* **12**, 148 (2020).
56. J. Li *et al*., EZH2-mediated H3K27 trimethylation mediates neurodegeneration in ataxia-telangiectasia. *Nat. Neurosci.* **16**, 1745–1753 (2013).
57. A. Chalkiadaki, L. Guarente, The multifaceted functions of sirtuins in cancer. *Nat. Rev. Cancer* **15**, 608–624 (2015).
58. E. F. Fang *et al*., Defective mitophagy in XPA via PARP-1 hyperactivation and NAD(+)/SIRT1 reduction. *Cell* **157**, 882–896 (2014).
59. S. A. Trammell *et al*., Nicotinamide riboside is uniquely and orally bioavailable in mice and humans. *Nat. Commun.* **7**, 12948 (2016).
60. R. W. Dellinger *et al*., Repeat dose NRPT (nicotinamide riboside and pterostilbene) increases NAD^+ levels in humans safely and sustainably: A randomized, double-blind, placebo-controlled study. *NPJ Aging Mech. Dis.* **3**, 17 (2017).
61. J. Ho, T. Tumkaya, S. Aryal, H. Choi, A. Claridge-Chang, Moving beyond P values: Data analysis with estimation graphics. *Nat. Methods* **16**, 565–566 (2019).